Bioactive Materials 6 (2021) 1839–1851

Contents lists available at ScienceDirect

Bioactive Materials

journal homepage: www.sciencedirect.com/journal/bioactive-materials

Simultaneous incorporation of PTH(1–34) and nano-hydroxyapatite into Chitosan/Alginate Hydrogels for efficient bone regeneration

Zhiyuan Zou [a,1], Le Wang [a,1], Zhifei Zhou [b], Qing Sun [c], Delong Liu [a,d], Yan Chen [a], Hao Hu [a], Yu Cai [e], Sixiong Lin [a], Zhengran Yu [a], Bizhi Tan [a], Wei Guo [a], Zemin Ling [a,*], Xuenong Zou [a,*]

[a] Guangdong Provincial Key Laboratory of Orthopaedics and Traumatology, Department of Spine Surgery, The First Affiliated Hospital of Sun Yat-sen University, Guangzhou 510080, China
[b] Key Laboratory of Functional Polymer Materials, Ministry of Education, Institute of Polymer Chemistry, College of Chemistry, Nankai University, Tianjin 300071, China
[c] Department of Pathology, Sun Yat-sen Memorial Hospital of Sun Yat-sen University, Guangzhou 510120, China
[d] Department of Orthopaedics, Hunan Provincial People's Hospital, Changsha 410002, China
[e] Institute of Chemical Biology, Shenzhen Bay Laboratory, Shenzhen, 518132, China

ARTICLE INFO

Keywords:
Parathyroid hormone
Hydrogels
Bone regeneration
Tissue engineering

ABSTRACT

Tissue regeneration based on the utilization of artificial soft materials is considered a promising treatment for bone-related diseases. Here, we report cranial bone regeneration promoted by hydrogels that contain parathyroid hormone (PTH) peptide PTH(1–34) and nano-hydroxyapatite (nHAP). A combination of the positively charged natural polymer chitosan (CS) and negatively charged sodium alginate led to the formation of hydrogels with porous structures, as shown by scanning electron microscopy. Rheological characterizations revealed that the mechanical properties of the hydrogels were almost maintained upon the addition of nHAP and PTH(1–34). In vitro experiments showed that the hydrogel containing nHAP and PTH(1–34) exhibited strong biocompatibility and facilitated osteogenic differentiation of rat bone marrow mesenchymal stem cells (rBMSCs) via the Notch signaling pathway, as shown by the upregulated expression of osteogenic-related proteins. We found that increasing the content of PTH(1–34) in the hydrogels resulted in enhanced osteogenic differentiation of BMSCs. Implantation of the complex hydrogel into a rat cranial defect model led to efficient bone regeneration compared to the rats treated with the hydrogel alone or with nHAP, indicating the simultaneous therapeutic effect of nHAP and PTH during the treatment process. Both the in vitro and in vivo results demonstrated that simultaneously incorporating nHAP and PTH into hydrogels shows promise for bone regeneration, suggesting a new strategy for tissue engineering and regeneration in the future.

1. Introduction

Bone defects resulting from congenital bone diseases, severe limb trauma, bone tumors, and infectious diseases cause major problems for patients and reduce their quality of life [1–3]. Unfortunately, the treatment of bone defects via conventional surgical operations is hindered by the limited transplantation materials [4 –6]. Autogenous transplantation, the gold standard method for bone therapy, is limited for the lack of sources of autografts [7,8], besides it also has a risk of infection, nerve damage and other postoperative complications [9]. To address these challenges, researchers have focused on the development of novel biomaterials with potential in tissue engineering and regeneration to facilitate bone regeneration [10–13]. Among synthetic biomaterials, hydrogels consisting of natural or synthetic polymers that exhibit excellent mechanical properties and biocompatibility are ideal scaffolds to emulate extracellular matrices for cell proliferation and differentiation [12,14–17], thus leading to broad utilization in bone regeneration. Thus far, many synthetic polymers, including poly (ethylene glycol), poly (vinyl alcohol), poly (acrylic acid), and poly (lactic acid), among others, have been utilized to develop hydrogels [18–21]. Natural polymers such as polypeptides, polysaccharides, and polynucleotides are alternative components for hydrogel scaffolds. Despite the progress achieved in the development of hydrogels over the past few decades, appropriate incorporation of therapeutics into

* Corresponding authors.
E-mail addresses: lingzm@mail2.sysu.edu.cn (Z. Ling), zxnong@hotmail.com, zouxuen@mail.sysu.edu.cn (X. Zou).
[1] These authors contributed equally to this work.

https://doi.org/10.1016/j.bioactmat.2020.11.021
Received 17 August 2020; Received in revised form 21 October 2020; Accepted 13 November 2020

hydrogels to efficiently promote bone regeneration is still challenging and limits the therapeutic efficacy of bone regeneration in vivo.

Parathyroid hormone (PTH) has among its targets were the cells of cartilage and bone. It mediates calcium and phosphate homeostasis, thus remodeling bone and cartilage growth [22,23]. The 1–34 amino acid fragment of PTH, i.e., PTH(1–34), is the active sequence responsible for the bone remodeling function of PTH and has been approved for use in the clinical treatment of osteoporosis or as a topical drug in the treatment of bone defects [24]. Low-dose and intermittent administration of PTH(1–34) leads to anabolic effects in bone regeneration and improvement of bone mineral density [25–27]. Recently, growing studies have demonstrated that systemic used or local delivery of PTH (1–34) to promote bone regeneration in bone defects [28–30]. Hence, incorporation of PTH(1–34) in hydrogels allows the preparation of biomaterials for bone regeneration. In addition, hydroxyapatite (HAP), a calcium phosphate bioceramic, is an essential component for bone regeneration [31–34]. Combining HAP with hydrogels enables emulation of the natural structures of bone and promotes bone regeneration [35–37]. The intrinsic mechanical properties of HAP and its interaction with bone tissues are intimately dependent on the size of HAP. Recent studies of HAP-based biomaterials have demonstrated that HAP with a nanoscale size, termed nano-HAP (nHAP), favors the cellular response and exhibits advanced performance in bone regeneration [38–40]. Despite the broad utilization of PTH(1–34) and nHAP in biomaterials, their combined therapeutic effects on bone regeneration remain unclear.

To develop biomaterials for bone regeneration beneficial from both PTH(1–34) and nHAP, here, we reported the simultaneous incorporation of PTH(1–34) and nHAP into hydrogels consisting of chitosan (CS) and sodium alginate (SA) and investigated the therapeutic effect on cranial bone regeneration. Both CS and SA are natural polysaccharides and exhibit strong biocompatibility [32,41–43]. CS is the N-deacetylation derivative of chitin and possesses positively charged amino groups [44], while alginate is composed of (1–4′)-linked β-D-mannuronic acid (M) and α-L-guluronic acid (G) moieties in various ratios and displays negatively charged carboxylic groups [45]. CS contains monomeric units comparable to glycosaminoglycans that associate with collagen fibers in the extracellular matrix and play an important role in cell adhesion [46,47]. Due to their oppositely charged groups, a combination of CS and SA allows for formation of robust hydrogels driven by electrostatic interactions [45,48,49]. The resulting hydrogels have been broadly utilized as scaffolds for therapeutic agents in tissue engineering and regeneration because of their facile preparation, biocompatibility, lack of immunogenicity, and biodegradability [48–50]. In our studies, we initially embedded nHAP into CS/SA hydrogels (Gel), leading to hybrid hydrogels with moderate mechanical properties suitable for drug scaffolds (Gel-nHAP). Subsequently, PTH(1–34) was added to the hybrid Gel-nHAP hydrogel at various concentrations in the range of 10–50 μg/mL, giving rise to the hydrogels Gel-nHAP-10 PTH, Gel-nHAP-20 PTH, and Gel-nHAP-50 PTH, to elucidate the dose-dependent therapeutic efficiency of PTH(1–34) on bone regeneration. We utilized the resulting hydrogels as culturing matrices for rat bone marrow mesenchymal stem cells (rBMSCs) to evaluate their biocompatibility and ability to modulate cell proliferation and differentiation. Furthermore, we found that it facilitated osteogenic differentiation of rBMSCs via the Notch signaling pathway. Eventually, the osteogenic efficacy of all the hydrogels was estimated using a rat skull defect model by coating the hydrogels on the defect area (as shown in Scheme 1).

2. Experimental section

2.1. Materials

PTH(1–34) was provided by ApexBio. CS (500–1000 kD) was purchased from Meryer (Shanghai) Chemical Technology Co., Ltd., and had a degree of deacetylation over 95%. SA was also purchased from Meryer (Shanghai) Chemical Technology Co., Ltd., with a molecular weight of 32–250 kD. Fluorescein isothiocyanate (FITC) was provided by Guangzhou Saiguo Biotech Co., Ltd. Polyethylene glycol (PEG400) was

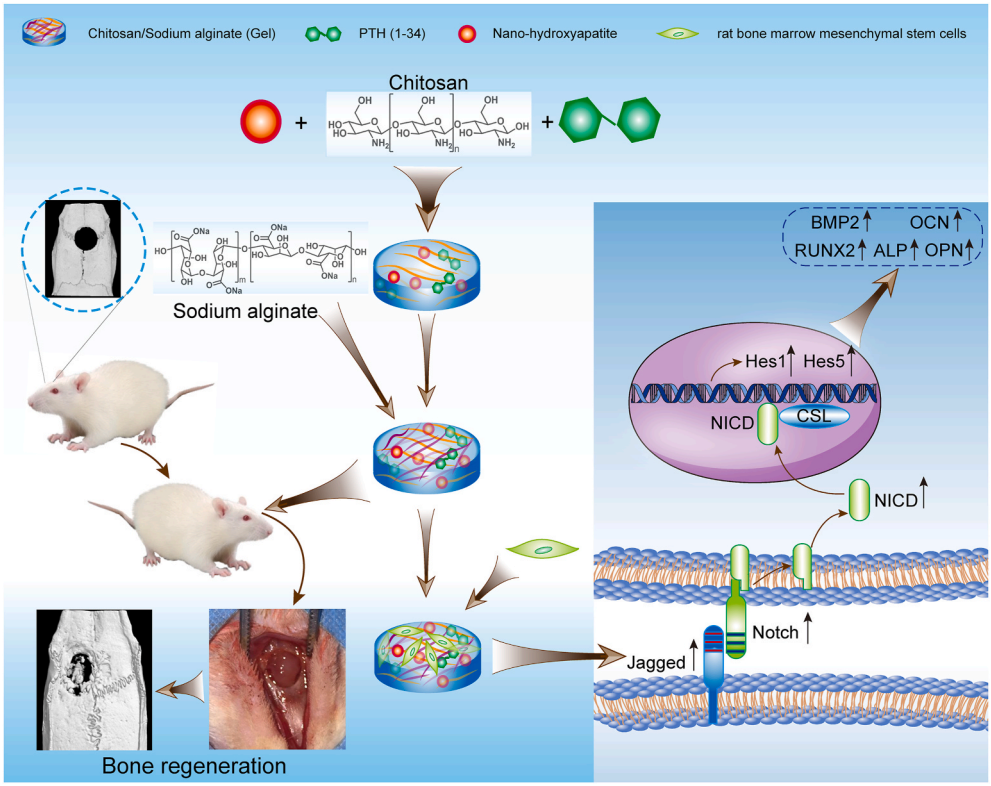

Scheme 1. Schematic illustration of preparation of the chitosan/sodium alginate (CA/SA) hydrogel simultaneously loaded with parathyroid hormone fragment PTH (1–34) and nano-hydroxyapatite for promoting cranial bone regeneration via the Notch signaling pathway.

purchased from TCI Chemicals (Shanghai) Co., Ltd. N,N-diisopropylethylamine (DIEA) was purchased from 3A Chemicals (Shanghai) Co., Ltd. Dimethyl sulfoxide (DMSO) was purchased from Shanghai BioLeaf Biotech Co., Ltd. N,N-dimethylformamide (DMF) was purchased from Tianjin Concord Chemical Technology Co., Ltd. nHAP (particle size: 60–80 nm) was purchased from Shanghai McLean Biochemical Co., Ltd. PBS (0.01 mol/L, pH 7.2–7.4) and ammonia hydroxide solution (25%) were purchased from Tianjin Wind Boat Chemical Reagent Technology Co., Ltd. Hydrochloric acid was purchased from Yongfei Chemical Reagent Co., Ltd. (Hebei, China). Fetal bovine serum (FBS) and antibiotic agents (penicillin/streptomycin, PS) were purchased from Gibco BRL (Invitrogen Co., USA).

2.2. Synthesis of FITC-labeled PTH(1–34) (FITC-PTH)

PTH(1–34) (10 mg, 0.0024 mmol) and FITC (1.4 mg) were dissolved in DMSO (2 mL). DIEA (2.6 mol/L) was added to the mixture, and the reaction solution was stirred in the dark for 18 h. After lyophilization to remove DMSO, the remaining mixture was dispersed in methanol to remove the unreacted FITC, and the solid was collected by centrifugation. After the sample was washed with DMF and methanol again, the solid was collected by centrifugation and re-dissolved in water (800 μL). Lyophilizing the solution led to FITC-PTH in a quantitative yield. The structure of FITC-PTH was characterized by MALDI-TOF mass spectrometry (Autoflex III TOF/TOF200, Bruker, Germany).

2.3. Preparation of hydrogels

Several stock solutions, including PTH(1–34) with a concentration of 2.5 or 5 mg/mL, FITC-PTH with a concentration of 2.5 or 5 mg/mL, nHAP in PEG400 with a concentration of 4% (w%), CS with a concentration of 2% (w%), and SA with a concentration of 5% (w%), were prepared to create the corresponding hydrogels.

Hydrogel CS/SA (Gel): The hydrogel CS/SA was prepared by adding the stock solution of CS (2% (w%), 1 mL) to the stock solution of SA (5% (w%), 1 mL). The hydrogel CS/SA, termed as Gel, was formed immediately upon mixing the solutions of CS and SA.

Hydrogel Gel-nHAP: To prepare hydrogel Gel-nHAP, the prepared stock solution of nHAP (4% (w%), 5 μL) was added to the stock solution CS (2% (w%), 1 mL). Addition of the stock solution of SA (5% (w%), 1 mL) to the mixed solution of nHAP and CS led to formation of hydrogel Gel-nHAP.

Hydrogels Gel-nHAP-x PTH: Hydrogels Gel-nHAP-x PTH [x denotes the content of PTH(1–34)] were prepared by adding stock solutions of nHAP and PTH(1–34) to that of CS and subsequently mixing in that of SA under an identical protocol for preparation of hydrogel Gel-nHAP. The final content of PTH(1–34) in the hydrogels was 10, 20, and 50 μg/mL, leading to the hydrogels Gel-nHAP-10 PTH, Gel-nHAP-20 PTH, and Gel-nHAP-50 PTH, respectively. To reduce the diluting effect of hydrogels, we used two stock solutions of PTH(1–34) at a concentration of 2.5 or 5 mg/mL, respectively, to prepare these hydrogels. To prepare hydrogel Gel-nHAP-10 PTH, the mixed solution of nHAP, PTH(1–34), and CS was prepared by adding the stock solutions of nHAP (4% (w%), 5 μL) and PTH(1–34) (2.5 mg/mL, 8 μL) to that of CS (2% (w%), 1 mL). To prepare hydrogel Gel-nHAP-20 PTH, the mixed solution of nHAP, PTH(1–34), and CS was prepared by adding the stock solutions of nHAP (4% (w%), 5 μL) and PTH(1–34) (2.5 mg/mL, 16 μL) to that of CS (2% (w%), 1 mL). To prepare hydrogel Gel-nHAP-50 PTH, the mixed solution of nHAP, PTH(1–34), and CS was prepared by adding the stock solutions of nHAP (4% (w%), 5 μL) and PTH(1–34) (5 mg/mL, 20 μL) to that of CS (2% (w%), 1 mL). Subsequently, adding the stock solution of SA (5% (w%), 1 mL) to the mixed solutions resulted in the hydrogels. In addition, the stock solution of unlabeled PTH(1–34) was replaced by that of FITC-PTH (1–34) during the preparation of the hydrogels utilized in the drug release assays.

2.4. Characterization of hydrogels

Rheological experiments: The rheological test of the hydrogels was carried out in oscillatory mode using a rheometer (AR 1500ex, TA Instruments, USA). During the experiments, the hydrogels were spread on a parallel plate (25 mm) and sealed with silicone oil to prevent solvent evaporation. A dynamic frequency scan in the range from 0.1 to 100 rad/s was used to record the storage and loss moduli G′ and G″. The stress amplitude and temperature were set as 0.1% and 25 °C, respectively.

Fourier transform infrared (FTIR) spectroscopy: The FTIR spectra of the hydrogels and individual components were obtained on an attenuated total reflection-FTIR spectroscope (Tensor II FTIR spectrometer, Bruker, Germany), and the scanned wavenumber was in the range of 4000 and 500 cm^{-1}.

Scanning electron microscopy (SEM): The hydrogels were coated on copper grids and dried under atmospheric conditions. The samples were sprayed with gold and detected by a scanning electron microscope (Zeiss Merlin Compact microscope, Germany) with an acceleration voltage of 5 kV.

2.5. Drug release assays

The release of PTH(1–34) from the Gel-nHAP-x PTH hydrogels was estimated by a fluorescence spectrometer (Agilent Cary Eclipse, Australia) by recording the emission of the fluorescein moiety excited at a wavelength of 495 nm. Prior to the assays, the hydrogel surface-located PTH(1–34) was gently washed away by PBS. The FITC-PTH-containing hydrogels were placed in dialysis tubes with a 10,000 MW cutoff. During the assays, 300 μL of PBS from outside of the tube was collected to monitor the fluorescence spectrum and returned to the sample after the measurement. This process was repeated as a function of time during the mentioned period to obtain the release kinetics of PTH(1–34).

2.6. rBMSC isolation, culture and identification

3 four-week-old male Sprague-Dawley (SD) rats were over-anesthetized with 3% pentobarbital sodium and euthanized. The rats were immersed in 75% ethanol for 15 min. The femurs and tibias of the rats were removed with sterilized instruments, and the bone marrow was removed. The obtained rBMSCs were suspended in α-Minimal Essential Medium (α-MEM) with 10% (v/v) FBS (Gibco, NY, USA) and 1% (v/v) PS (Gibco, NY, USA) in a 5% CO_2 incubator at 37 °C. The culture medium was changed every 2–3 days. The rBMSCs were passaged when in the cell culture dish reached 70–80%. Cells at passages 3 to 5 were used in the following experiments. Before use, these cells were analyzed by flow cytometry (CytoFLEX, Beckman Coulter, CA, USA) based on CD29, CD90, CD34, and CD45. In brief, a 200 μL suspension containing 1 million cells was added to 5 μL of FITC-labeled anti-rat CD29 (Abcam, Britain), PacificBlue BDHorizon®V450 (V450)-labeled anti-rat CD45 (Abcam, Britain) and phycoerythrin (PE)-labeled anti-rat CD90 and CD34 (Abcam, Britain) to incubate for 15 min. The labeled cells were sorted by flow cytometry (CytoFLEX, Beckman Coulter, CA, USA) and analyzed by Cell Quest analysis software (BD, USA). The ability of rBMSCs to undergo osteogenic differentiation was evaluated by Alizarin red staining, and the adipogenic differentiation potential was confirmed by oil red O staining; these analyses were performed after 21 days.

2.7. CCK-8 cell proliferation assay

The CCK-8 cell proliferation assay was performed according to the manufacturer's instructions. Briefly, rBMSCs were inoculated at a cell density of 5×10^4 cells/mL into 12-well plates covered with different kinds of hydrogels. A group without hydrogel was defined as a negative

control group. After 1, 3, and 5 days of incubation, Cell Counting Kit-8 (CCK-8; Dojindo Molecular Technologies, Inc., Japan) equivalent to 10% of the total volume of the culture medium was added to each well of the 12-well plates and incubated for 4 h in a cell culture chamber placed away from light. Then, 100 μL of culture medium was transferred to 96-well plates, and the absorbance at a wavelength of 450 nm was measured to evaluate the proliferation of rBMSCs cultured on different groups. The absorbance was measured at a wavelength of 450 nm using a microplate reader (Multiskan MK3, Thermo Fisher Scientific, USA) and was then used to evaluate the proliferation of rBMSCs cultured in the different groups. The final result is that the wavelength of the experimental group minus the wavelength of the blank group is expressed as the optical density (OD).

2.8. Annexin V/PI staining by flow cytometry

The cells were cultured on a hydrogel scaffold for 48 h, and the apoptotic cells were quantified by Annexin V/PI double staining reagent (Invitrogen, USA). The rBMSCs from the different scaffolds and negative control groups (cell and culture medium group) were harvested and washed twice with cold PBS. Then, the cells were resuspended in 400 μL of 1X Binding Buffer, and 5 μL of FITC Annexin V and 5 μL of PI were added. The cells were gently vortexed and incubated for 15 min at room temperature (25 °C) in the dark. The preparations were analyzed by flow cytometry (BD FACSAria III, USA).

2.9. Immunofluorescence

Then rat BMSCs were inoculated with the control, Gel-nHAP scaffold, and Gel-nHAP-PTH scaffold at 2×10^4 cells/cm^2 and cultured with α-MEM supplemented with 10% FBS for 7 days. The specimens from each group were washed with phosphate-buffered saline (PBS) solution three times, fixed with 4% paraformaldehyde for 20 min, and then washed three times with PBS. Subsequently, after incubation with 0.5% Triton X-100 in PBS for 20 min, the samples were blocked in PBS solution containing 1% bovine serum albumin (BSA) for 30 min.

Next, the samples were incubated with the primary antibodies anti-Notch1 (1:200, Abcam, USA) and anti-osteocalcin (OCN) (1:200, Abcam, USA) overnight at 4 °C. Then, the secondary antibodies conjugated to FITC or TRITC were incubated at 37 °C for 1 h. Finally, the nucleus was stained with DAPI, and the cytoskeleton was stained with F-actin. The images were observed and collected with a fluorescence microscope (Leica DMi8, Germany). Five visual fields were randomly selected using the image analysis software Image-Pro Plus to measure the intensity of OCN and Notch1.

2.10. Western blot analysis

Next, rBMSC cells were cultured on different scaffolds for 14 days. The proteins were extracted using RIPA buffer (Sigma-Aldrich), and a Pierce BCA Protein Assay Kit (Thermo Scientific) was used to determine the total protein concentration. The same amount of lysates was separated by SDS-PAGE (Beyotime, China) and transferred onto a PVDF membrane (Millipore, USA). The membrane was blocked in TBST solution containing 5% skim milk (BD, USA) and incubated at 4 °C overnight with the specific primary antibodies anti-BMP2 (1:1000, Abcam, USA), anti-Runx2 (1:1000, Abcam, USA), anti-OCN (1:1000, Abcam, USA), anti-Notch1 (1:500, Abcam, USA), anti-Jagged1 (1:500, Abcam, USA), anti-NICD1 (1:1000, Abcam, USA), and anti-GAPDH (1:2500, Abcam, USA), and then incubated with the appropriate secondary antibodies. The band signals were detected using Pierce ECL Plus Western blotting Substrate (Thermo Scientific, USA). The band gray level was quantified using ImageJ software.

2.11. RNA isolation and quantitative real-time PCR

Next, the rBMSCs were cultured in plates covered with different types of hydrogel scaffolds and the control, and the expression of osteogenic genes was analyzed at 14 days. Total RNA was isolated from the samples using TRIzol reagent (TaKaRa, Japan) according to the manufacturer's protocol. Reverse transcription was performed with PrimeScript RT Master Mix (TaKaRa, Japan). The expression of ALP, OCN, Runx2, OPN, Notch1, Jagged1, Hes1, Hes5, and GAPDH was analyzed by real-time PCR using TB Green Premix Ex *Taq*II (TaKaRa, Japan). The results were normalized to the expression of GAPDH. The primer sequence of each gene is shown in Table 1. Analysis of each gene in the samples was performed in triplicate.

2.12. In vivo study

All animal feeding and surgical procedures complied with the relevant laws and were authorized by the Ethics Committee at The First Affiliated Hospital of Sun Yat-sen University. Thirty 12-week-old male SD rats with a weight ranging from 300 to 350 g were used in this study. All rats were purchased from the Southern Medical University Experiment Animal Center (Guangzhou, China). All animals were given food and water ad libitum and housed at room temperature with a consistent light/dark cycle. All rats were anesthetized intraperitoneally with 3% pentobarbital sodium (30 mg/kg). After cutting the cranium hair with a hair knife, a longitudinal incision was made in the middle of the skull to cut the skin and subcutaneous tissue in turn. Next, an electric trephine drill was used to create a full-thickness circular defect of 5 mm in diameter in the parietal area of the rat cranium. Then, Gel-nHAP, Gel-nHAP-10 PTH, Gel-nHAP-20 PTH, and Gel-nHAP-50 PTH scaffolds were randomly used to fill the cranial defect in the rats. The group without any hydrogel scaffold was the negative control group. Then, the soft tissue and skin were sutured layer by layer. The animals were injected with streptomycin (0.125 mg) and penicillin (0.1 mg) once a day for 3 days after the operation. Ketorolac was used to relieve pain at 1 mg/kg and then once a day for 3 days.

At 12 weeks after surgery, six rats from each group were sacrificed by an intraperitoneal injection of overdose pentobarbital. The extracted rat skull samples were fixed in 10% neutral-buffered formalin (Leagene, China) for 24 h and then scanned by microcomputed tomography (micro-CT) and subjected to histological analysis and immunohistochemistry.

2.13. Micro-CT

After the rats were sacrificed, each cranium sample was scanned

Table 1
Primer sequences for related genes.

Gene	Primer Sequences (5′–3′)
Alkaline phosphatase (ALP)	Forward primer: TGCAGGATCGGAACGTCAAT
	Reverse primer: GAGTTGGTAAGGCAGGGTCC
Osteocalcin (OCN)	Forward primer: TCCCTCTCTCTGCCTCGAAA
	Reverse primer: GGGCTGTCTGGGATTGAACA
Osteopontin (OPN)	Forward primer: GGGATCGCTGAAGGCATCAA
	Reverse primer: CAGCCGTCAAAGGCTTCAAA
RUNX2	Forward primer: CACAAGTGCGGTGCAAACTT
	Reverse primer: AATGACTCGGTTGGTCTCGG
Notch1	Forward primer: TTGGTCCGAGGGCATCTCTA
	Reverse primer: ACAGAGCTTGGGAACGGAAG
Jagged1	Forward primer: CTGCTTGAATGGGGGTCACT
	Reverse primer: CACGATTGTAGCATTGGGCG
Hes1	Forward primer: CAACACGACACCGGACAAAC
	Reverse primer: CGGAGGTGCTTCACTGTCAT
Hes5	Forward primer: GTGGAGATGCTCAGTCCCAA
	Reverse primer: TCAATGCTGCTGTTGATGCG
GAPDH	Forward primer: AGTGCCAGCCTCGTCTCATA
	Reverse primer: GGGTTTCCCGTTGATGACCA

using a micro-CT system (SkyScan1276 Micro-CT, Bruker, Germany) with 85 kV, 200 μA, and 1 mm aluminum filtration. The results were reconstructed with NRecon software (Bruker, Germany). Three-dimensional analyses were carried out using CTvox software. The bone volume/tissue volume (BV/TV) and Bone mineral density (BMD) were calculated by CTAn analysis software.

2.14. Histological analysis

After micro-CT scanning, rat calvarial samples were decalcified in 10% ethylenediaminetetraacetic acid (EDTA, Leagene, China) solution for 2 weeks. The samples were dehydrated by relevant processing procedures of graded alcohol series, embedded in paraffin, and used to generate 4-μm-thick sections. Bone regeneration was analyzed by hematoxylin and eosin (H&E) and Masson's trichrome staining. The stained sections of samples were observed by microscopy (Leica DMi8, Germany).

2.15. Immunohistochemistry (IHC)

Histological sections of the samples were deparaffinized in xylene and then hydrated in descending alcohol followed by water. The sections were placed in citrate buffer and heated in an autoclave for 10 min for antigen retrieval. After the sections were blocked with hydrogen peroxide, they were incubated with anti-OCN (1:200, Abcam, USA) primary antibodies at room temperature for 1 h. After the samples were washed with wash buffer, the appropriate secondary antibodies were added. Diaminobenzidine was used for visualization, followed by

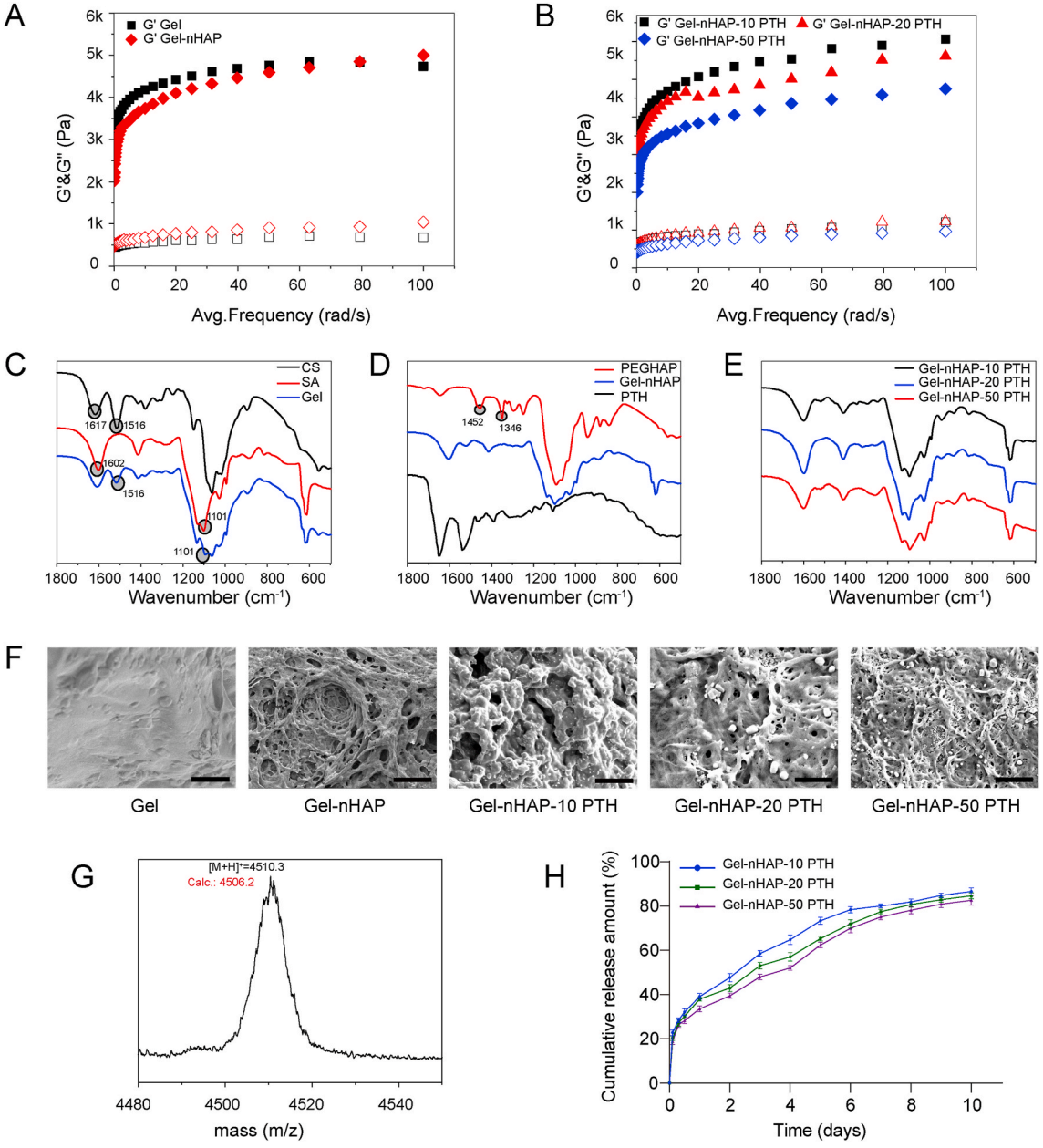

Fig. 1. (A and B) Storage (G′) and loss (G″) moduli of the hydrogels estimated by rheological studies, in which hydrogels CS/SA Gel and Gel-nHAP were shown in (A), whereas hydrogels Gel-nHAP-10 PTH, Gel-nHAP-20 PTH, and Gel-nHAP-50 PTH were shown in (B). (C–E) Fourier transform infrared spectra of CS, SA, Gel (C), PEG-nHAP, Gel-nHAP, PTH (D), Gel-nHAP-10 PTH, Gel-nHAP-20 PTH, and Gel-nHAP-50 PTH (E). (F) Scanning electron microscopic images of hydrogels Gel, Gel-nHAP, Gel-nHAP-10 PTH, Gel-nHAP-20 PTH, and Gel-nHAP-50 PTH. Scale bars: 10 μm. (G) Mass spectrum of FTIC-labeled PTH(1–34). (H) Cumulative percentage release of PTH(1–34) from different hydrogel scaffolds during a period of 10 days.

counterstaining with hematoxylin. Following dehydration, the slides were coverslipped.

2.16. Statistical analysis

All data analyses were performed using SPSS 23.0 software (IBM, USA). Data are presented as the mean ± standard deviations (SD) of at least three independent experiments. Statistical analysis was performed using one-way ANOVA with Tukey's post hoc test. $P < 0.05$ was considered significant: *$P < 0.05$; **$P < 0.01$.

3. Results and discussion

3.1. Characterization of the hydrogel scaffolds

We carried out rheological experiments to confirm the formation of the hydrogels and characterize their mechanical properties (Fig. 1A and B). Under the frequency-dependent oscillatory shear model, all the prepared hydrogels had storage moduli (G′) that were higher than the corresponding loss moduli (G″ viscous response) by almost one order of magnitude over the entire frequency range, indicating the formation of hydrogels [50]. Upon reaching the plateau, all the hydrogels exhibited a storage modulus over 4 kPa, suggesting the moderate mechanical property of the hydrogels and their utilization as scaffolds for bone regeneration. The addition of nHAP to CS/SA Gels resulted in a slight change in the mechanical properties, primarily due to the low level of nHAP in the hybrid hydrogel Gel-nHAP. Interestingly, we found that increasing the content of PTH(1–34) in the hydrogels reduced the storage moduli of the hydrogels, leading to the following order of the stiffness of the hydrogels: Gel-nHAP-10 PTH > Gel-nHAP-20 PTH > Gel-nHAP-50 PTH. The decrease in the stiffness of the hydrogels containing a high amount of PTH(1–34) is potentially attributed to the disruption of the electrostatic interactions between two polymers arising from the peptides.

The structural components of the hydrogels were confirmed by FTIR spectroscopy (Fig. 1C, D, and E). While CS exhibited conventional absorbance bands at 1617 and 1516 cm^{-1} associated with the N–H vibration, SA showed bands at 1602 and 1102 cm^{-1} arising from the vibration of carboxylic groups. The FTIR spectrum of the CS/SA Gel displayed absorbance bands corresponding to the vibration of the N–H and carboxylic groups, indicating the coexistence of CS and SA within the hydrogel. In addition, the characteristic absorbance bands of nHAP and PTH(1–34) were not observed in the FTIR spectra of the corresponding hydrogels, predominately due to the low content of these two components in the hydrogels compared to the natural polymers. The morphology of the hydrogels was characterized by SEM (Fig. 1F). While the SEM image of the CS/SA Gel showed relatively untangled networks and stiff structures, the addition of nHAP and PTH(1–34) to the hydrogels led to the formation of entangled soft fibers with porous structures. The crystal structure of nHAP was observed in the image of Gel-nHAP, demonstrating the retained structures of nHAP in the hydrogels.

SEM images also revealed that increasing the content of PTH(1–34) in the hydrogels thinned the present entangled fibers. Nevertheless, the porous structure of the hydrogels potentially facilitates drug release from the scaffolds and their association with cells.

3.2. In vitro drug release

We estimated the drug PTH(1–34) release from the hydrogels Gel-nHAP-10 PTH, Gel-nHAP-20 PTH, and Gel-nHAP-50 PTH with FITC-PTH by monitoring the fluorescence intensity of FITC (Fig. 1H). The chemical structure of FITC-PTH was confirmed by mass spectrometry. As shown in Fig. 1G, the calculated molecular weight of the covalently linked FITC and PTH(1–34) was observed in the MALDI-TOF MS spectrum, confirming the attachment of a single FITC moiety to PTH(1–34) and the formation of FITC-PTH. We further monitored the release of PTH (1–34) from the hydrogels through a dialysis setup. The release profiles of PTH(1–34) from the hydrogels Gel-nHAP-10 PTH, Gel-nHAP-20 PTH, and Gel-nHAP-50 PTH showed a constant release of PTH(1–34) over 10 days, suggesting the robust stability of the hydrogels under physiological conditions for a long period and their usage as drug release scaffolds. The release kinetics of PTH(1–34) from the three hydrogels did not display a significant difference, potentially due to the low occupied density of the pores of the hydrogels.

3.3. Identification of rBMSCs

We extracted rBMSCs from SD rats, and the third passage cells were analyzed by flow cytometry to confirm the characteristic markers on the surface of the rBMSCs (Fig. 2A): CD29 (+), CD90 (+), CD34 (−), and CD45 (−). Multilineage differentiation of rBMSCs was induced by osteogenic (Fig. 2B) and adipogenic media (Fig. 2C). These results indicate that the cells we extracted from the rat bone marrow were mainly rBMSCs.

3.4. Proliferation and viability of the rBMSCs cultured on hybrid hydrogel scaffolds

We used CCK-8 assays to evaluate the effect of the hybrid hydrogel scaffolds and the control on cell proliferation. As shown in Fig. 3A, on the first day, there was no significant difference in the cell proliferation performance between the various hydrogels because cell proliferation requires time. However, with the extension of time, the proliferation of cells became obvious. In a certain range, the increase in the concentration of PTH(1–34) significantly promoted cell proliferation. The results showed that the hybrid hydrogels containing PTH(1–34) had good biocompatibility, were nontoxic and strongly promoted cell proliferation. On day 5, there were significant differences among the groups ($P < 0.01$).

In addition, we used flow cytometry to detect the effects of different kinds of materials on apoptosis to provide a reference basis for its practical application. After the cells were cultured on hydrogel scaffolds for 48 h, the results showed that the apoptosis rates of the control group, Gel-nHAP group, Gel-nHAP-10 PTH group, Gel-nHAP-20 PTH group, and Gel-nHAP-50 PTH group were (Q3) 1.51%, 1.91%, 1.82%, 1.74%, and 1.68%, respectively, and the necrosis rate (Q2) was 1.24%, 0.81%, 2.87%, 1.54%, and 1.22%, respectively (Fig. 3B–F). These results indicated that all hydrogel scaffolds had a little effect on cell apoptosis and necrosis, and the hybrid hydrogels had good biocompatibility, cytocompatibility and good biological function.

3.5. Osteogenic differentiation of BMSCs in the hybrid hydrogel scaffolds in vitro

Ideal bone repair materials should enhance the osteogenic differentiation of cells. To reveal the effect of hydrogel scaffolds on the osteogenic differentiation of rBMSCs in vitro, we seeded cells on the control and the Gel-nHAP, Gel-nHAP-10 PTH, Gel-nHAP-20 PTH and Gel-nHAP-50 PTH scaffolds. After the cells were cultured on the hydrogels for 14 days, the expression of osteogenic markers was analyzed by Western blots. The results showed that both the Gel-nHAP group and the Gel-nHAP-PTH group performed better than control group ($P < 0.01$, Fig. 4A and B), the hydrogels containing PTH(1–34) could better promote the expression of osteogenic proteins (Runx2, BMP2, OCN) than the Gel-nHAP hydrogel and the control, and the osteogenic effect was more obvious with the increase in the content of PTH(1–34). Additionally, these results suggested that PTH(1–34) in the scaffolds can promote the osteogenic differentiation of rBMSCs.

It was reported that the administration of PTH(1–34) during the recovery of transcortical lesions (experimentally drilled in the rat femur) accelerates the succession of stages in the repair of skeletal lesions, i.e.

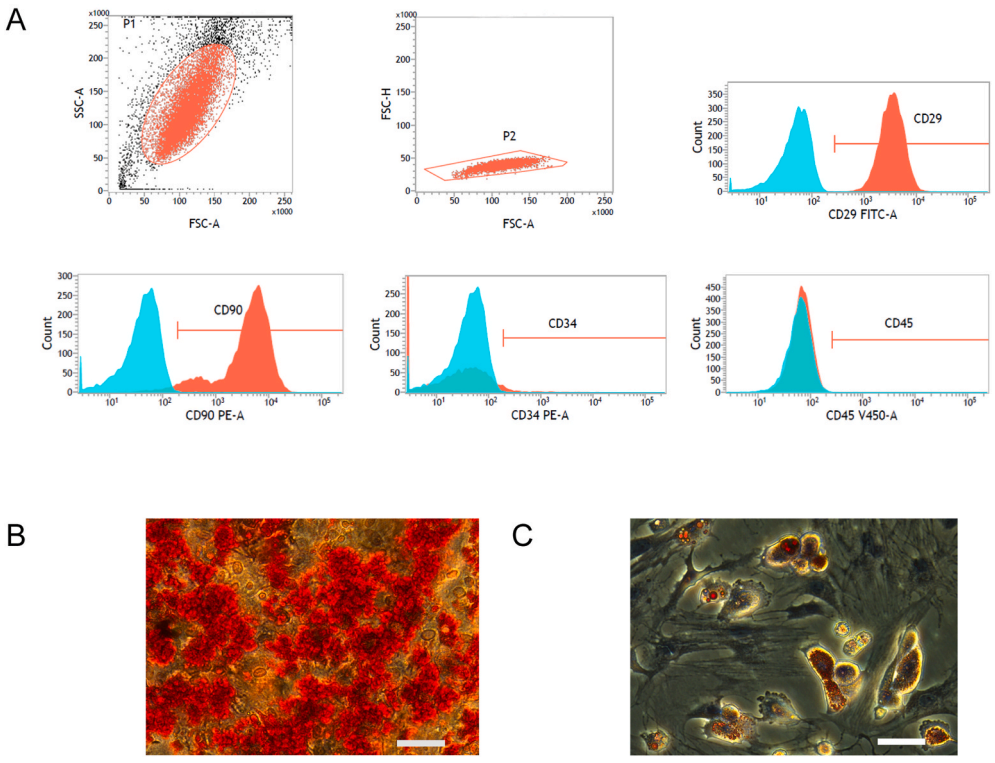

Fig. 2. (A) Flow cytometric analyses of cell surface markers CD29, CD90, CD34, and CD45 of rBMSC cells cultured with α-MEM supplemented with 10% FBS. (B and C) The ability of rBMSC to differentiate into the osteogenic, adipogenic lineages as confirmed through Alizarin red staining (B) and oil Red O staining(C). Scale bar: 50 μm.

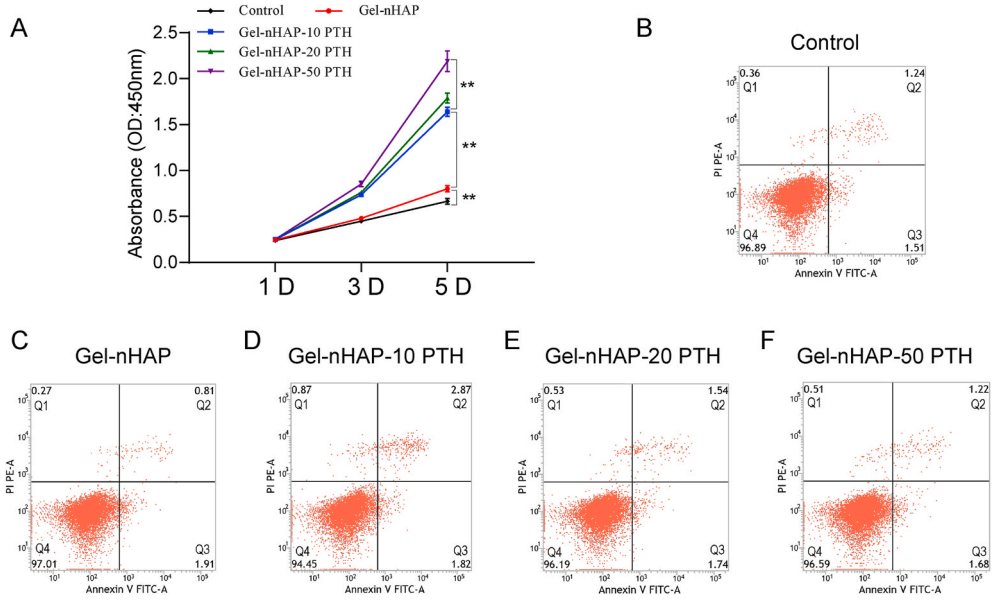

Fig. 3. (A) Viability of rBMSC cells of cultured on hydrogels Gel-nHAP, Gel-nHAP-10 PTH, Gel-nHAP-20 PTH, and Gel-nHAP-50 PTH evaluated by CCK-8 assay at 1, 3, and 5 days. (B–F) Cell apoptosis quantified by flow cytometry of rBMSC cells of cultured on culture medium (B) or hydrogels Gel-nHAP (C), Gel-nHAP-10 PTH (D), Gel-nHAP-20 PTH (E), and Gel-nHAP-50 PTH (F) for 48 h. Data are expressed as the mean ± SD. **P < 0.01.

anticipates the occurrence of dynamic osteogenesis involved in the production of good quality bone, with respect to the phase of static osteogenesis, occurring at the onset of the reparative sequence [51].

Real-time PCR showed that the expression of osteogenesis-related genes in the Gel-nHAP groups and the Gel-nHAP-PTH groups were higher than that in the control group (Fig. 5A–D). The mRNA levels of osteogenic markers, including ALP, OCN, OPN, and Runx2, on the rBMSCs inoculated in the hybrid Gel-nHAP-PTH hydrogels was higher than that in the Gel-nHAP groups, suggesting that the Gel-nHAP-PTH scaffolds could effectively promote osteogenic differentiation of rBMSCs. With the increase in PTH(1–34) concentration, the mRNA expression levels of osteogenic markers increased.

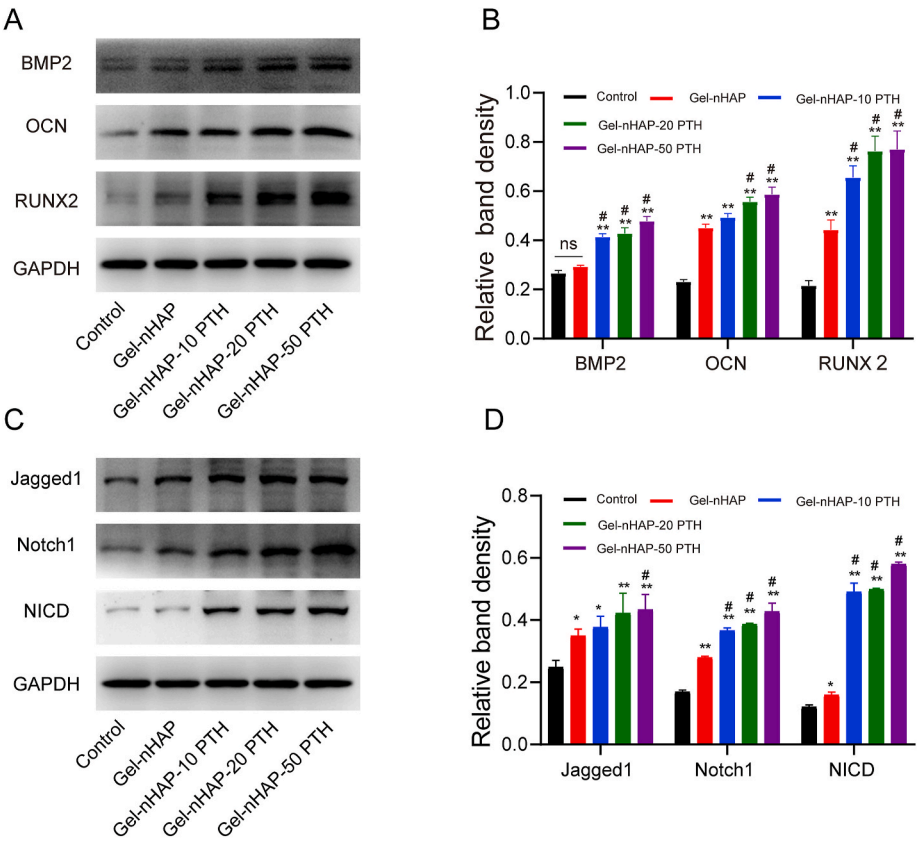

Fig. 4. (A and B) Western blotting of osteogenic proteins BMP2, OCN and RUNX2 (A) and their quantitative analyses (B) expressed by rBMSC cells cultured on different scaffolds for 14 days. (C and D) Western blotting of the proteins Jagged1, Notch1, and NICD involved in the Notch signaling pathway of rBMSC cells cultured on different scaffolds for 14 days (C) and their quantitative analysis (D). Data are expressed as the mean ± SD. $^{**}p < 0.01$ and $^{*}p < 0.05$, comparison between control group and hydrogel groups; $^{\#}p < 0.05$, comparison among hydrogels. ns stands for no significant difference.

3.6. The Notch signaling pathway promotes osteogenic differentiation

The Notch signaling pathway is an evolutionarily conserved intercellular signaling pathway [52], which plays an important role in the regulation of cell differentiation and cell fate and participates in the regulation of adult stem cell differentiation [52,53]. This pathway has been shown to play a key role in the proliferation and osteogenic differentiation of stem cells [54,55]. A previous study showed that calcium phosphate scaffolds could induce osteogenic differentiation through the typical Notch signaling pathway [56]. Therefore, we hypothesized that the Gel-nHAP-PTH scaffolds could promote osteogenic differentiation of rBMSCs by upregulating the Notch signaling pathway. We verified this hypothesis by Western blot and real-time PCR analyses. rBMSCs were inoculated in the control, Gel-nHAP scaffolds, and Gel-nHAP-PTH scaffolds and cultured in α-MEM supplemented with 10% FBS. After 14 days, the protein expression in the Notch signaling pathway was detected by Western blotting. The results showed that compared with the control group, the Notch1, Jagged1, NICD, Hes1, and Hes5 levels in the Gel-nHAP-PTH and Gel-nHAP groups were significantly increased ($P < 0.05$). The expression of proteins related to the Notch signaling pathway was higher in the Gel-nHAP-PTH group than the Gel-nHAP group (Fig. 4C and D).

In addition, we further detected the expression of related genes in the Notch signaling pathway by real-time PCR. We compared the transcription levels of related genes in the Notch signaling pathway, Notch1, Jagged1, Hes1, and Hes5, and the results showed (Fig. 5E–H) that the Jagged1 and Hes5 expression levels in the Gel-nHAP-PTH (20,50) group were higher than those in the control group ($P < 0.05$) and the Gel-nHAP groups ($P < 0.05$). The Hes1 expression level was higher in the Gel-nHAP-PTH group than the control group and Gel-nHAP groups ($P < 0.05$). In addition, the mRNA levels of Notch1 were higher in the Gel-nHAP-PTH (50) group than the control group and Gel-nHAP groups ($P < 0.05$). The Notch1 expression levels in the Gel-nHAP-20 PTH group were significantly increased compared with the control group.

We further analyzed the expression of osteogenic proteins in the Notch signaling pathway such as Notch1 and OCN by immunofluorescence after 7 days of BMSC culturing in α-MEM containing 10% FBS on the scaffolds and control groups.

Notch1 staining was localized in the cytoplasm (Fig. 6A), while the Notch1 signal was observed in the Gel-nHAP-PTH cells (Fig. 6A and C). In addition, the protein level of OCN was significantly higher in the Gel-nHAP-PTH group than the Gel-HAP and control groups (Fig. 6B and D).

In summary, our results indicated that the Gel-nHAP-PTH scaffold induced activation of the Notch signaling pathway and promoted an increase in osteogenic proteins and genes to improve osteogenic differentiation.

3.7. Hybrid hydrogel scaffolds regenerate bone in vivo

To further evaluate the effect of hybrid hydrogel on bone regeneration in vivo, we implanted Gel-nHAP, Gel-nHAP-10 PTH, Gel-nHAP-20 PTH, and Gel-nHAP-50 PTH scaffolds into rat cranial defects, with blank groups without hydrogels serving as the control group, to observe bone reactivation effects (Fig. 7A and B). When the hydrogel was implanted, we cut the hydrogel into a circular 5 mm with a thickness of 1.5 mm, just filling the size of the rat cranial defect.

Twelve weeks later, after the rats were killed by overdose injection, the cranial defects were collected and reconstructed with micro-CT for three-dimensional reconstruction (Fig. 7C and D). As shown in Fig. 7C, in the blank group (without any scaffolds), a large cavity defect still existed, indicating that there was little bone regeneration and only a small amount of fibrous tissue. The effect of a hybrid hydrogel containing PTH(1–34) on repairing cranial defects in rats was better than in the Gel-nHAP group. In addition, with the increase in content of PTH (1–34) in the hybrid hydrogels, the effect on the repair of bone defects became more obvious. Quantitative evaluation of newborn bone growth

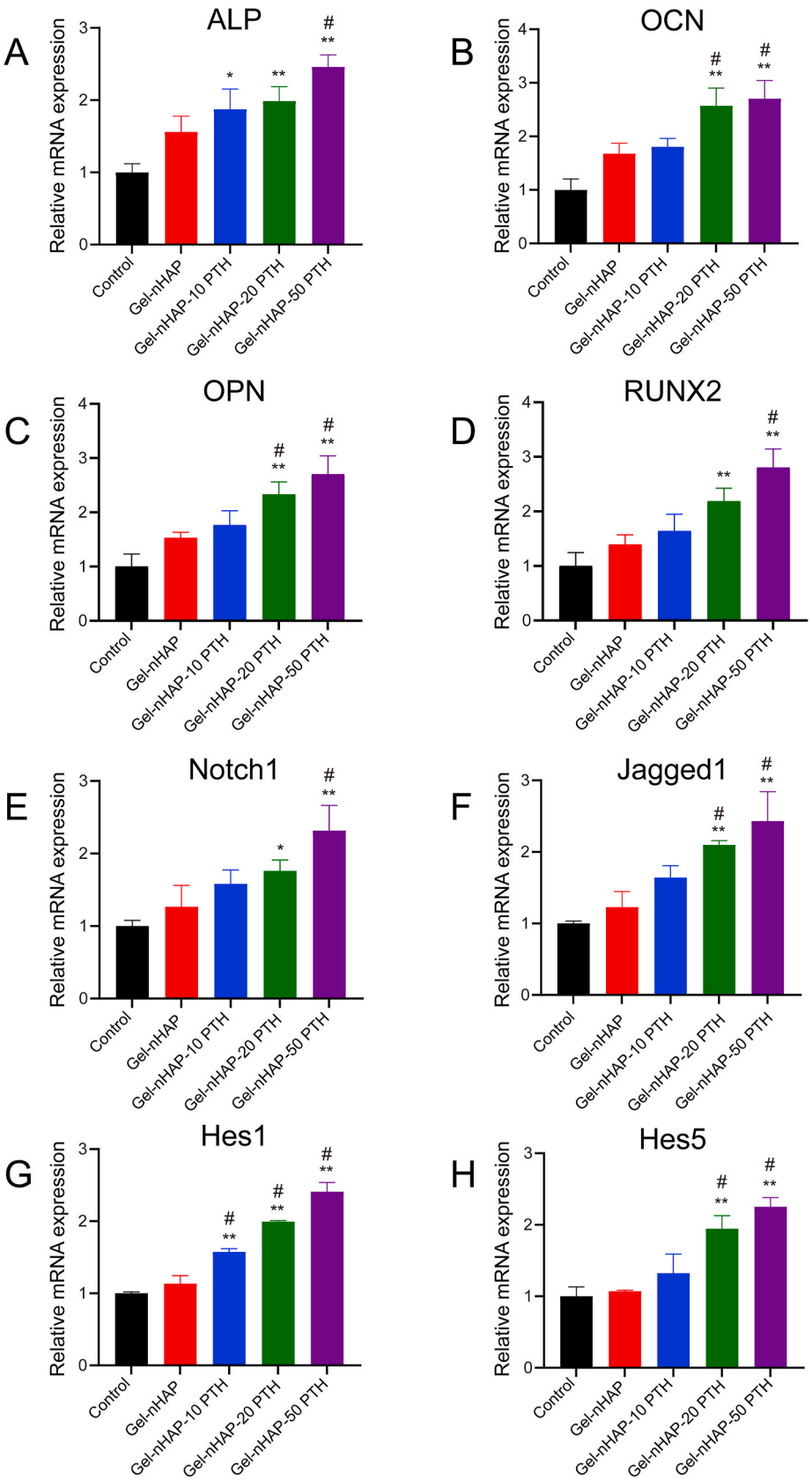

Fig. 5. Expression of osteogenic genes ALP (A), OCN (B), OPN (C), and RUNX2 (D), and the corresponding genes Notch1 (E), Jagged1 (F), Hes1 (G), and Hes5 (H) in the Notch signaling pathway by rBMSC cells after incubation on different scaffolds after 14 days estimated by real-time PCR. Data are expressed as the mean ± SD. $^{**}p < 0.01$ and $^{*}p < 0.05$, comparison between control group and hydrogel groups; $^{\#}p < 0.05$, comparison between different hydrogels.

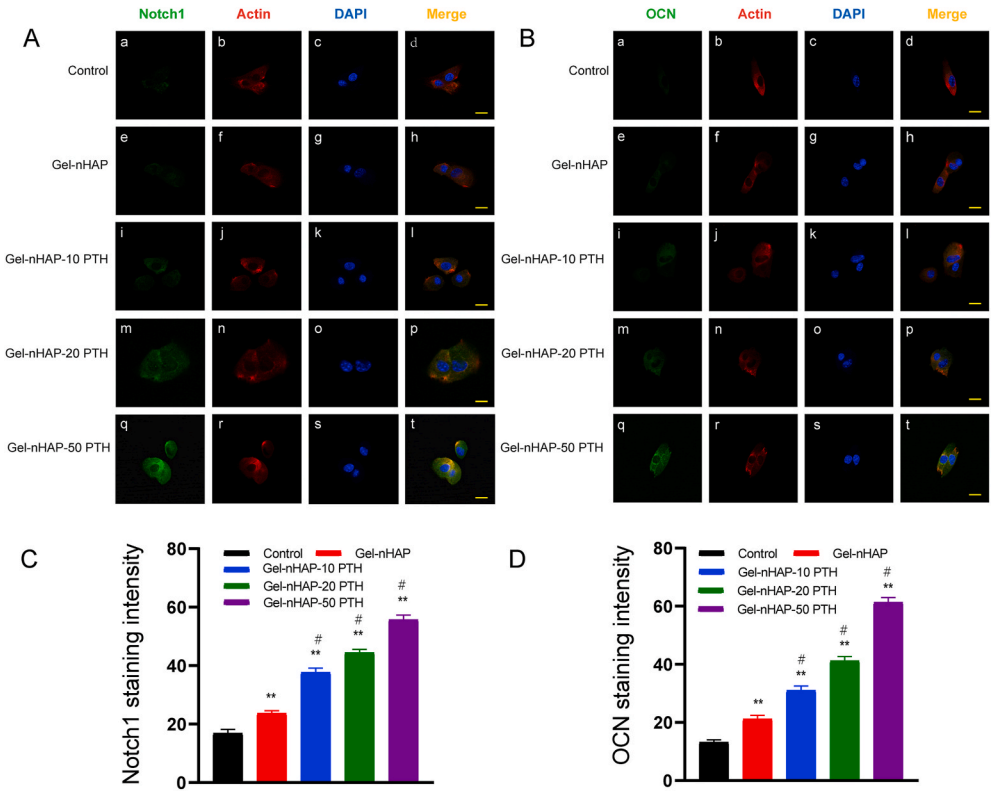

Fig. 6. Immunofluorescence images of rBMSC cells cultured on different groups and stained by OCN, Notch1, F-Actin, DAPI. A (a, e, i, m, q) expression of Notch1 (green), A (b, f, j, n, r) Cell skeleton staining with F-Actin (red). A (c, g, k, o, s) Nuclear staining with DAPI (blue). A(d, h, l,p, t) Merged images. B (a, e, i, m, q) Expression of OCN (green) of rBMSCs on scaffolds and control group. B (b, f, j, n, r) Cell skeleton staining with F-Actin (red). B (c, g, k, o, s) Nuclear staining with DAPI (blue). B (d, h, l,p, t) Merged images. (C) Relative intensity of Notch1of rat BMSCs on different groups. (D) Relative intensity of OCN of rBMSCs on different groups. Scale bars, 20 μm. Data are expressed as the mean ± SD. $^{**}p < 0.01$ and $^{*}p < 0.05$, comparison between control group and hydrogel groups; $^{\#}p < 0.05$, comparison between different hydrogels.

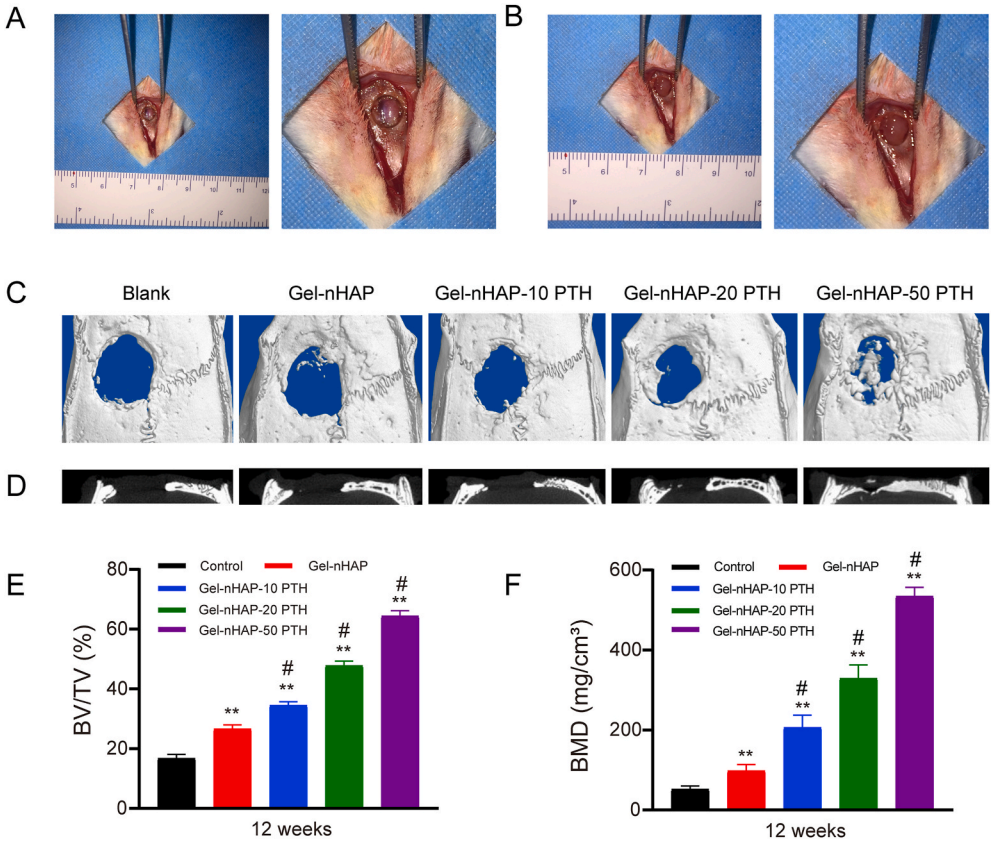

Fig. 7. (A) 12-week-old male SD Rat cranial defects model and larger image; (B)The scaffolds were implanted in the cranial defect of rat and larger image; (C) Micro-computed tomography images of cranial defects implanted by different scaffolds or left empty 12 weeks postoperative; (D) Micro-CT scanning showed the coronal image of the five groups; (E) The bone volume/tissue volume (BV/TV) and Bone mineral density (BMD) were calculated by CTAn analysis software. The group without any scaffolds implanted was set as the control, also is the blank group. Data are expressed as the mean ± SD. $^{**}p < 0.01$ and $^{*}p < 0.05$, comparison between control group and hydrogel groups; $^{\#}p < 0.05$, comparison between different hydrogels.

using CTAn analysis software, BV/TV, and bone mineral density (BMD) were performed. Growth was best in the Gel-nHAP-50 PTH group, followed by the Gel-nHAP-20 PTH and Gel-nHAP-10 PTH groups, which showed better results than the group without filling and the group filled with Gel-nHAP scaffold ($P < 0.01$). The growth of new bone was superior in the Gel-nHAP group compared with the blank group ($P < 0.01$) (Fig. 7E). As shown by BMD (Fig. 7F), BMD was significantly increased in the Gel-nHAP-50 PTH group, followed by the Gel-nHAP-20 PTH, Gel-nHAP-10 PTH, Gel-nHAP group, and the control group with the lowest bone mineral density. Our results showed that the bone mineral density of hydrogel containing PTH was higher compared with the hydrogel group without PTH, and it increased correspondingly with the increase in PTH content.

H&E and Masson's trichrome staining further histologically verified the formation and maturity of new bone. As shown by H&E staining images (Fig. 8A), no inflammatory reaction or necrosis was observed in any of the groups. The control group was not filled with hydrogel, and fibrous connective tissue was mainly observed. There was no obvious new bone formation. A small amount of new bone tissue appeared in the Gel-nHAP group, and new bone appeared in the hybrid hydrogel groups containing PTH, especially the Gel-nHAP-50 PTH group. The color of the new bone tissue was slightly whiter than the host bone. The color of mature bone was similar to the host bone, and it easily combined with the host bone. Masson's trichrome staining showed that collagen fibers, ossified tissue, mucus, and cartilage were blue; muscle fibers, cellulose, and red cells were red; and nuclei were blue-black. As shown in Fig. 8B, in the blank group, very few collagen fibers and ossified tissues formed at the defect site. In the Gel-nHAP-PTH group, there were more collagen fibers and ossification tissues than in the Gel-nHAP group. With the increase in PTH(1–34) content in the hybrid hydrogel scaffolds, blue staining of collagen fibers and ossification tissues increased correspondingly.

The results were confirmed by immunohistochemical staining of OCN, and the positive staining of new bone and osteoblasts was significantly improved in the Gel-nHAP-PTH scaffolds compared with the Gel-nHAP scaffolds and blank control (Fig. 8C). Therefore, the Gel-nHAP-PTH scaffold could significantly promote bone regeneration and repair of bone defects. In addition, immunohistochemical staining further confirmed the positive effect of PTH(1–34) in osteogenesis and new bone formation. The results showed that hybrid hydrogel scaffolds loaded with PTH(1–34) could promote the regeneration of bone tissue and had a good repair effect on bone defects.

It has been reported that PTH has dual effects on bone formation and bone resorption by regulating RANKL/OPG ratios [57]. High-dose and continuous infusion can lead to bone absorption [58], while intermittent low-dose administration of PTH can increases bone formation [59,60], as well as, local application of PTH has been indicated to promote osteogenesis [61]. Although intermittent PTH1-34 treatment has a good function to increase bone formation, it may increase the incidence of osteosarcoma because of systemic treatment [24]. Therefore, local delivery of PTH may stimulate osteogenesis but decrease the side effect of systemic treatment. Many studies had been reported that the osteogenic effect of materials containing PTH used in bone defects is better than that of materials without PTH [62,63], which is consistent with our experimental results.

It is noteworthy that nano-hydroxyapatite itself showed good bone conductivity and can promote bone regeneration [64–66]. When PTH (1–34) was combined with nHAP, these characteristics were more obvious. CS and SA are both natural polysaccharides and have strong biocompatibility. Our experimental results showed that the

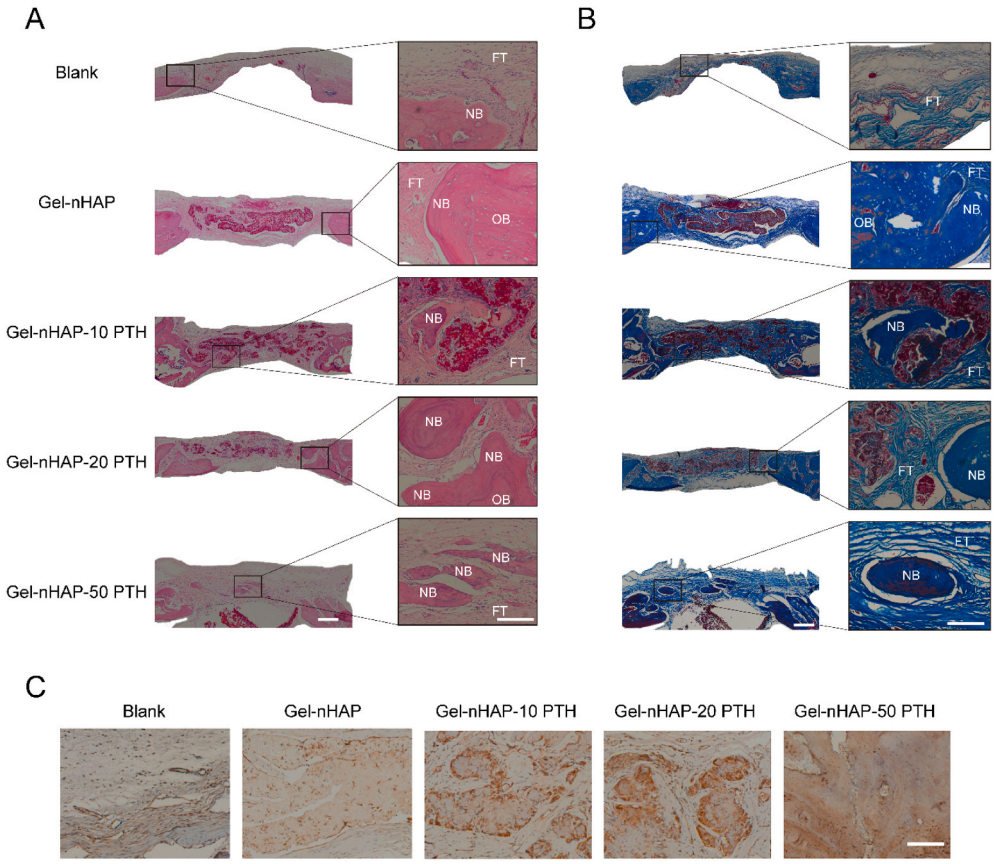

Fig. 8. Bone regeneration in a cranial defect after 12 weeks. (a) Representative images of H&E staining (scale bar: left=500μm, right=100μm); (B) Masson's trichrome staining images. (Scale bar: left=500μm, right= 100μm); (C) Immunohistochemical staining of OCN. (scale bar, 100μm). (NB: New bone, OB: original bone, FT: fibrous tissue).

Gel-nHAP-PTH scaffold can promote bone regeneration. Within a certain range, PTH(1–34) has a dose-dependent effect on bone regeneration.

In our study, recovery of the rat cranial defect was incomplete, which might be explained as follows. The time was relatively short, resulting in an insufficient period to promote bone regeneration. Moreover, a small amount of PTH(1–34) was used, so increasing the amount may promote complete regeneration of the cranial defect. Furthermore, our results could be due to matching of various components in our hybrid hydrogel. In future analyses, we will optimize the design of hybrid hydrogels.

The present study has several limitations. First, we used rat bone marrow mesenchymal stem cells, which are primary cells, without additional cell lines for further verification. Further research should include testing different cell lines of each cell and their differences in bone regeneration. Second, no long-term observation of the rat cranial defect was performed, and 12 weeks is a relatively short duration. In the future, it will be possible to observe the osteogenic effect for 6 months or longer. In addition, we can also attempt to study the osteogenic effect of the limb long bone defect, which will complement and contrast with the study of bone defects.

4. Conclusions

In summary, we designed novel Gel-nHAP-PTH hybrid hydrogel scaffolds and used them for local bone regeneration for the first time. The nanofibers and porous structure of the Gel-nHAP-PTH scaffolds enhance cell adhesion and show good binding with bone tissue to promote bone regeneration. With the increase in PTH(1–34), the scaffold nanofibers became finer, which is more conducive to bone regeneration. The Gel-nHAP-PTH scaffold has high biocompatibility and can significantly promote bone regeneration. Interestingly, the Gel-nHAP-PTH scaffold significantly promoted osteogenic activity via the Notch signaling pathway and increased the expression levels of osteogenic proteins such as BMP-2, OCN and RUNX2. In addition, in vivo experiments showed that the Gel-nHAP-PTH hybrid hydrogel scaffold significantly promoted bone regeneration. The Gel-nHAP-PTH scaffold was superior to the Gel-nHAP scaffold in promoting proliferation, osteogenesis of rat BMSCs and bone regeneration. This study demonstrated that simultaneously incorporating nHAP and PTH(1–34) into hydrogels represents a promising strategy for bone regeneration, thus serving as a new strategy for tissue engineering and regeneration in the future.

CRediT authorship contribution statement

Zhiyuan Zou: Conceptualization, Methodology, Data curation, Writing - original draft. **Le Wang:** Conceptualization, Methodology, Writing - original draft. **Zhifei Zhou:** Data curation. **Qing Sun:** Writing - original draft. **Delong Liu:** Writing - original draft. **Yan Chen:** Writing - original draft. **Hao Hu:** Writing - original draft. **Yu Cai:** Writing - original draft. **Sixiong Lin:** Data curation. **Zhengran Yu:** Investigation. **Bizhi Tan:** Investigation. **Wei Guo:** Writing - original draft. **Zemin Ling:** Conceptualization, Writing - review & editing. **Xuenong Zou:** Supervision, Validation, Writing - review & editing.

Declaration of competing interest

The authors declare no conflict of interest.

Acknowledgements

This work was supported by the National Natural Science Foundation of China (No. U1601220, 32071341, 31430030), Natural Science Foundation of Guangdong Province (2017A030308004), Natural Science Foundation of Guangzhou City (201804020011),The Science and Technology Project of Guangdong province (2018A050506021), and The International Science and Technology Cooperation Project of Science and Technological Bureau of Guangzhou Huangpu District (2018GH16).

References

[1] B. Fan, Z. Guo, X. Li, et al., Electroactive barium titanate coated titanium scaffold improves osteogenesis and osseointegration with low-intensity pulsed ultrasound for large segmental bone defects, Bioactive Materials 5 (2020) 1087–1101.
[2] C.B. Danoux, D. Barbieri, H. Yuan, et al., In vitro and in vivo bioactivity assessment of a polylactic acid/hydroxyapatite composite for bone regeneration, Biomatter 4 (2014), e27664.
[3] S. Mobini, B. Hoyer, M. Solati-Hashjin, et al., Fabrication and characterization of regenerated silk scaffolds reinforced with natural silk fibers for bone tissue engineering, J. Biomed. Mater. Res. (2013) 2392–2404.
[4] Z.X.H. Lim, B. Rai, T.C. Tan, et al., Autologous bone marrow clot as an alternative to autograft for bone defect healing, Bone Joint Res 8 (2019) 107–117.
[5] R. Dimitriou, E. Jones, D. McGonagle, et al., Bone regeneration: current concepts and future directions, BMC Med. 9 (2011) 66.
[6] J. Henkel, M.A. Woodruff, D.R. Epari, et al., Bone regeneration based on tissue engineering conceptions - a 21st century perspective, Bone Res 1 (3) (2013) 216–248.
[7] X. Baia, S. Lü, H. Liu, et al., Polysaccharides based injectable hydrogel compositing bio-glass forcranial bone repair, Carbohydr. Polym. 175 (2017) 557–564.
[8] W.G. De Long, T.A. Einhorn, K. Koval, et al., Bone grafts and bone graft substitutes in orthopaedic trauma surgery. A critical analysis, J Bone Joint Surg Am 89 (3) (2007) 649–658.
[9] R.V. da Silva, C.A. Bertran, E.Y. Kawachi, et al., Repair of cranial bone defects with calcium phosphate ceramic implant or autogenous bone graft, J. Craniofac. Surg. 18 (2) (2007) 281–286.
[10] Y. Ji, M. Wang, W. Liu, et al., Chitosan/nHAC/PLGA microsphere vehicle for sustained release of rh BMP-2 and its derived synth.etic oligopeptide for bone regeneration, J. Biomed. Mater. Res. 105 (6) (2017) 1593–1606.
[11] L. Chen, C. Wu, S. Chen, et al., Biomimetic mineralizable collagen hydrogels for dynamic bone matrix formation to promote osteogenesis, J. Mater. Chem. B. 8 (2020) 3064–3075.
[12] S. Stratton, N.B. Shelke, K. Hoshino, et al., Bioactive polymeric scaffolds for tissue engineering, Bioactive Materials 1 (2016) 93–108.
[13] A.R. Armiento, L.P. Hatt, G.S. Rosenberg, et al., Functional biomaterials for bone regeneration: a lesson in complex biology, Adv. Funct. Mater. (2020) 1909874.
[14] J. Sun, X. Zhao, W.R.K. Illeperuma, et al., Highly stretchable and tough hydrogels, Nature 489 (2012) 133–136.
[15] Y.H. Tsou, J. Khoneisser, P.C. Huang, et al., Hydrogel as a bioactive material to regulate stem cell fate, Bioactive Materials 1 (2016) 39–55.
[16] J. Chen, X. Zou, Self-assemble peptide biomaterials and their biomedical applications, Bioactive Materials 4 (2019) 120–131.
[17] G. Wang, X. Cao, H. Dong, et al., A hyaluronic acid based injectable hydrogel formed via photo-crosslinking reaction and thermal-induced diels-alder reaction for cartilage tissue engineering, Polymers 10 (2018) 949.
[18] F.D. Sala, M. Biondi, D. Guarnieri, et al., Mechanical behavior of bioactive poly (ethylene glycol) diacrylate matrices for biomedical application. Journal of the Mechanical Behavior of Biomedical Materials, J Mech Behav Biomed Mater 110 (2020) 103885.
[19] H. Zhang, H. Xia, Y. Zhao, Poly(vinyl alcohol) hydrogel can autonomously self-heal, ACS Macro Lett. 1 (2012) 1233–1236.
[20] G. Sennakesavan, M. Mostakhdemin, L.K. Dkhar, et al., Acrylic acid/acrylamide based hydrogels and its properties-A review, Polym. Degrad. Stabil. 180 (2020) 109308.
[21] A. Basu, K.R. Kunduru, S. Doppalapudi, et al., Poly(lactic acid) based hydrogels, Adv. Drug Deliv. Rev. 107 (2016) 192–205.
[22] M.N. Wein, H.M. Kronenberg, Regulation of bone remodeling by parathyroid hormone, Cold Spring Harb Perspect Med 8 (2018) a031237.
[23] J. Huang, D. Lin, Z. Wei, et al., Parathyroid hormone derivative with reduced osteoclastic activity promoted bone regeneration via synergistic bone remodeling and angiogenesis, Small (2020) 1905876.
[24] C. Berg, K. Neumeyer, P. Kirkpatrick, Teriparatide, Nat. Rev. Drug Discov. 2 (2003) 257–258.
[25] Y. Yoshioka, E. Yamachika, M. Nakanishi, et al., Intermittent parathyroid hormone 1-34 induces oxidation and deterioration of mineral and collagen quality in newly formed mandibular bone, Sci. Rep. 9 (1) (2019) 8041.
[26] Y. Tang, H. Xia, L. Kang, et al., Effects of intermittent parathyroid hormone 1–34 administration on circulating mesenchymal stem cells in postmenopausal osteoporotic women, Med. Sci. Mon. Int. Med. J. Exp. Clin. Res. 25 (2019) 259–268.
[27] K. Ogura, T. Iimura, Y. Makino, et al., Short-term intermittent administration of parathyroid hormone facilitates osteogenesis by different mechanisms in cancellous and cortical bone, BoneKEy Rep. 5 (2016) 7–14.
[28] L. Jiang, W. Zhang, L. Wei, et al., Early effects of parathyroid hormone on vascularized bone regeneration and implant osseointegration in aged rats, Biomaterials 179 (2018) 15–28.
[29] S.J. Wojda, I.A. Marozas, K.S. Anseth, et al., Thiol-ene hydrogels for local delivery of PTH for bone regeneration in critical size defects, J. Orthop. Res. 38 (2020) 536–544.
[30] M. Dang, A.J. Koh, X. Jin, et al., Local pulsatile PTH delivery regenerates bone defects via enhanced bone remodeling in a cell-free scaffold, Biomaterials 114 (2017) 1–9.

[31] C. Fang, Y. Lin, F. Lin, et al., Biomimetic synthesis of nanocrystalline hydroxyapatite composites: therapeutic potential and effects on bone regeneration, Int. J. Mol. Sci. 20 (2019) 6002.
[32] Q. Wang, Y. Tang, Q. Ke, et al., Magnetic lanthanum-doped hydroxyapatite/chitosan scaffolds with endogenous stem cell-recruiting and immunomodulatory properties for bone regeneration, J. Mater. Chem. B. 8 (2020) 5280–5292.
[33] W. Su, X. Ma, Z. Sun, et al., RhBMP-2 and concomitant rapid material degradation synergistically promote bone repair and regeneration with collagen–hydroxyapatite nanocomposites, J. Mater. Chem. B 6 (2018) 4338–4350.
[34] J. Son, J. Kim, K. Lee, et al., DNA aptamer immobilized hydroxyapatite for enhancing angiogenesis and bone regeneration, Acta Biomater. 99 (2019) 469–478.
[35] A.R. Bastos, L.P. da Silva, F.R. Maia, et al., Lactoferrin-hydroxyapatite containing spongy-like hydrogels for bone tissue engineering, Materials 12 (2019) 2074.
[36] M. Rivas, L.J.D. Valle, C. Alemán, et al., Peptide self-assembly into hydrogels for biomedical applications related to hydroxyapatite, Gels 5 (1) (2019) 14.
[37] A. Timofejeva, D. Loca, Hydroxyapatite/polyvinyl alcohol composite hydrogels for bone and cartilage tissue engineering, Key Eng. Mater. 762 (2018) 54–58.
[38] L. Zheng, X. Jiang, X. Chen, et al., Evaluation of novel in situ synthesized nano-hydroxyapatite/collagen/alginate hydrogels for osteochondral tissue engineering, Biomed. Mater. 9 (6) (2014), 065004.
[39] Y. Liu, J. Gu, D. Fan, Fabrication of high-strength and porous hybrid scaffolds based on nano-hydroxyapatite and human-like collagen for bone tissue regeneration, Polymers 12 (2020) 61.
[40] Y. Cho, M. Quan, N. Kang, et al., Strategy for enhancing mechanical properties and bone regeneration of 3D polycaprolactone kagome scaffold: nano hydroxyapatite composite and its exposure, Eur. Polym. J. 134 (2020) 109814.
[41] H.L. Kim, G.Y. Jung, J.H. Yoon, et al., Preparation and characterization of nano-sized hydroxyapatite/alginate/chitosan composite scaffolds for bone tissue engineering, Mater Sci Eng C Mater Biol Appl 54 (2015) 20–25.
[42] J. Prakash, D. Prema, K.S. Venkataprasanna, et al., Nanocomposite chitosan film containing graphene oxide/hydroxyapatite/gold for bone tissue engineering, Int. J. Biol. Macromol. 154 (2020) 62–71.
[43] P. Nezhad-Mokhtari, M. Akrami-Hasan-Kohal, M. Ghorbani, An injectable chitosan-based hydrogel scaffold containing gold nanoparticles for tissue engineering applications, Int. J. Biol. Macromol. 154 (2020) 198–205.
[44] D. Algul, A. Gokce, A. Onal, et al., In vitro release and in vivo biocompatibility studies of biomimetic multilayered alginate-chitosan/β-TCP scaffold for osteochondral tissue, J. Biomater. Sci. Polym. Ed. 27 (5) (2016) 431–440.
[45] J.A. Hunt, R. Chen, T. Veen, et al., Hydrogels for tissue engineering and regenerative Medicine, J. Mater. Chem. B. 2 (2014) 5319–5338.
[46] X. Ji, W. Yang, T. Wang, et al., Coaxially electrospun core/shell structured poly(L-lactide) acid/chitosan nanofibers for potential drug carrier in tissue engineering, J. Biomed. Nanotechnol. 9 (10) (2013) 1672–1678.
[47] A. Anitha, S. Sowmya, P.T. Sudheesh Kumar, et al., Chitin and chitosan in selected biomedical applications, Prog. Polym. Sci. 39 (2014) 1644–1667.
[48] J. Sun, H. Tan, Alginate-based biomaterials for regenerative medicine applications, Materials 6 (2013) 1285–1309.
[49] T. Wu, J. Huang, Y. Jiang, et al., Formation of hydrogels based on chitosan/alginate for the delivery of lysozyme and their antibacterial activity, Food Chem. 240 (2018) 361–369.
[50] Y. Zhang, H. Zhang, Q. Zou, et al., An injectable dipeptide–fullerene supramolecular hydrogel for photodynamic antibacterial therapy, J. Mater. Chem. B. 6 (2018) 7335–7342.
[51] F. Cavani, M. Ferretti, A. Smargiassi, C. Palumbo, PTH(1-34) effects on repairing experimentally drilled holes in rat femur: novel aspects – qualitative vs. quantitative improvement of osteogenesis, J. Anat. 230 (2017) 75–84.
[52] J.T. Zieba, Y. Chen, B.H. Lee, et al., Notch signaling in skeletal development, homeostasis and pathogenesis, Biomolecules 10 (2020) 332.
[53] C. Siebel, U. Lendahl, Notch signaling in development, tissue homeostasis, and disease, Physiol. Rev. 97 (4) (2017) 1235–1294.
[54] R.A. Lawal, X. Zhou, K. Batey, et al., The Notch ligand Jagged1 regulates the osteoblastic lineage by maintaining the osteoprogenitor pool, J. Bone Miner. Res. 32 (6) (2017) 1320–1331.
[55] Y. Tian, Y. Xu, T. Xue, et al., Notch activation enhances mesenchymal stem cell sheet osteogenic potential by inhibition of cellular senescence, Cell Death Dis. 8 (2017) e2595.
[56] Y. Wang, J. Pan, Y. Zhang, et al., Wnt and Notch signaling pathways in calcium phosphate-enhanced osteogenic differentiation: a pilot study, J. Biomed. Mater. Res. Part B 107 (2019) 149–160.
[57] L. Qin, L.J. Raggatt, N.C. Partridge, Parathyroid hormone: a double-edged sword for bone metabolism, Trends Endocrinol. Metabol. 15 (2004) 60–65.
[58] B.C. Silva, J.P. Bilezikian, Parathyroid hormone: anabolic and catabolic actions on the skeleton, Curr. Opin. Pharmacol. 22 (2015) 41–50.
[59] G.J. Pettway, J.A. Meganck, A.J. Koh, et al., Parathyroid hormone mediates bone growth through the regulation of osteoblast proliferation and differentiation, Bone 42 (2008) 806–818.
[60] Y. Ohkawa, K. Tokunaga, N. Endo, Intermittent administration of human parathyroid hormone (1-34) increases new bone formation on the interface of hydroxyapatitecoated titanium rods implanted into ovariectomized rat femora, J. Orthop. Sci. 13 (2008) 533–542.
[61] M.J. Horwitz, M.B. Tedesco, S.M. Sereika, et al., A 7-day continuous infusion of PTH or PTHrP suppresses bone formation and uncouples bone turnover, J. Bone Miner. Res. 26 (2011) 2287–2297.
[62] R.E. Jung, D.L. Cochran, O. Domken, et al., The effect of matrix bound parathyroid hormone on bone regeneration, Clin. Oral Implants Res. 18 (2007) 319–325.
[63] I. Arrighi, S. Mark, M. Alvisi, et al., Bone healing induced by local delivery of an engineered parathyroid hormone prodrug, Biomaterials 30 (2009) 1763–1771.
[64] P. Kubasiewicz-Ross, J. Hadzik, J. Seeliger, et al., New nano-hydroxyapatite in bone defect regeneration: a histological study in rats, Ann. Anat. 213 (2017) 83–90.
[65] M. Meskinfam, S. Bertoldi, N. Albanese, et al., Polyurethane foam/nano hydroxyapatite composite as a suitable scaffold for bone tissue regeneration, Mater Sci Eng C Mater Biol Appl (2018) 130–140.
[66] A. Tae Young, J.H. Kang, D.J. Kang, et al., Interaction of stem cells with nano hydroxyapatite-fucoidan bionanocomposites for bone tissue regeneration, Int. J. Biol. Macromol. 93 (2016) 1488–1491.